Hindawi Publishing Corporation
International Journal of Antennas and Propagation
Volume 2016, Article ID 8485305, 11 pages
http://dx.doi.org/10.1155/2016/8485305

Research Article

A Parasitic Array Receiver for ISAR Imaging of Ship Targets Using a Coastal Radar

Fabrizio Santi and Debora Pastina

Department of Information Engineering, Electronics and Telecommunications, University of Rome "La Sapienza", Via Eudossiana 18, 00184 Rome, Italy

Correspondence should be addressed to Fabrizio Santi; santi@diet.uniroma1.it

Received 15 April 2016; Accepted 12 June 2016

Academic Editor: Michelangelo Villano

The detection and identification of ship targets navigating in coastal areas are essential in order to prevent maritime accidents and to take countermeasures against illegal activities. Usually, coastal radar systems are employed for the detection of vessels, whereas noncooperative ship targets as well as ships not equipped with AIS transponders can be identified by means of dedicated active radar imaging system by means of ISAR processing. In this work, we define a parasitic array receiver for ISAR imaging purposes based on the signal transmitted by an opportunistic coastal radar over its successive scans. In order to obtain the proper cross-range resolution, the physical aperture provided by the array is combined with the synthetic aperture provided by the target motion. By properly designing the array of passive devices, the system is able to correctly observe the signal reflected from the ships over successive scans of the coastal radar. Specifically, the upper bounded interelement spacing provides a correct angular sampling accordingly to the Nyquist theorem and the lower bounded number of elements of the array ensures the continuity of the observation during multiple scans. An *ad hoc* focusing technique has been then proposed to provide the ISAR images of the ships. Simulated analysis proved the effectiveness of the proposed system to provide top-view images of ship targets suitable for ATR procedures.

1. Introduction

The monitoring and protection of the coastal area are a primary task to improve the situation awareness in the maritime domain and considerably efforts have been made over the last years to improve the levels of safety and security by using available monitoring and control systems [1]. Ground-based, airborne, and spaceborne radar sensors play a fundamental role in the framework of maritime surveillance, due to their capability to detect, track, and possibly image ship targets autonomously and continuatively, night and day and even in hard meteorological conditions. As well as the employment of active radar systems, over the last years a number of studies concerning passive radar systems for marine applications have been conducted, essentially motivated by the well-known benefits of passive radars. Indeed, since only the receiver has to be designed and developed, such kind of systems is extremely of low cost if compared to conventional active systems. Typically, they have small dimensions and hence can be deployed in place where heavy conventional radars cannot be. In addition, since they do not emit any waves, they provide increased antijamming capabilities as well as reduced environmental pollution. In the field of maritime surveillance, different opportunity illuminators have been proved able to increase safeguarding coastlines, such as geostationary telecommunication satellites [2, 3], digital terrestrial television transmitters [4, 5], and WiMAX [6] and cell phone [7] base stations. On the other hand, since the transmitted waveforms are designed for different purposes, they are not optimal for radar applications. A different solution is to exploit the signals emitted by opportunistic radar.

Traditionally, the control of the traffic along the coast is accomplished by the use of a ground-based radar system having its antenna rotating with a speed of 10–30 rpm, azimuth beamwidth of 0.4–2°, and a range resolution of few meters. Moreover, they are often equipped with a second antenna

able to receive the Automatic Identification System (AIS) signal transmitted by cooperative vessels, which provides to the marine traffic coordinator their unique identifiers, as well as their courses and speeds. However, information as much as possible has to be gathered about noncooperative targets, which may be involved in illegal activities such as piracy, human smuggling, or terrorist actions. Furthermore, small-sized vessels often do not carry an AIS transponder, and they could potentially increase the insurgence of accidents. Automatic Target Recognition (ATR) procedures greatly help maritime safety and security organizations, and often they rely on radar images. Nevertheless, the antenna angle resolution of a coastal radar is not sufficient to provide an image suitable for the recognition of the detected ship. However, by exploiting the well-known principle of the Inverse Synthetic Aperture Radar (ISAR) [8, 9], radar images with sufficient resolution for recognition can be obtained and employed in ATR procedures [10]. In this work, we consider a parasitic radar system that exploits the friendly emissions of a coastal radar in order to provide ISAR images of ship targets.

As is well known, ISAR technique exploits the ship movements with respect to the stationary radar to produce an image of the ship itself. Usually, the rotational motion of the ship around its center of gravity induced by the sea waves is exploited to produce the Doppler gradient needed to achieve the desired cross-range resolution. However, in the case of low sea-state this ship rotation can be negligible or not sufficient for the formation of the ISAR image. In such a case, it is of interest to develop an ISAR mode relying on the translational motion only. As typical ship velocities are limited to about twenty knots (about 10 m/s), ship reflected signals have to be integrated over a long integration time to achieve an ISAR image with reasonable resolution. While the radar antenna rotates, it illuminates the target for a time interval given by the time-on-target. Typical values of the scan rates and azimuth beam widths for a coastal radar entail times-on-target of tens of milliseconds, certainly too short for imaging purposes. Nevertheless, the target is again illuminated after a time interval equal to the time needed to the antenna to complete a scan, and by exploiting the signal reflected by the ship over successive scans, a processing time long enough for the ISAR process can be obtained. On the other hand, the usual values of the scan rates of the coastal radar give rise to sampling frequencies considerably lower than the Doppler bandwidth and therefore the coastal radar by itself cannot carry out a proper sampling of the azimuth signal.

The solution proposed here to achieve a proper sampling of the signal in the azimuth domain is to use an array of passive sensors located near the coast receiving the signal transmitted by the coastal radar over its successive scans (and otherwise not involved in the imaging activity) and reflected by the ship. The proper configuration of the array parameters, that is, number of elements and their reciprocal distance, is therefore linked to the parameters of the coastal radar as well as the target motion (a preliminary assessment of the system has been presented in [11]). Then, by jointly exploiting the physical aperture provided by the parasitic array and the synthetic aperture based on the target motion, a proper processing of the data provides a well-focused image to be efficiently employed in ATR procedures.

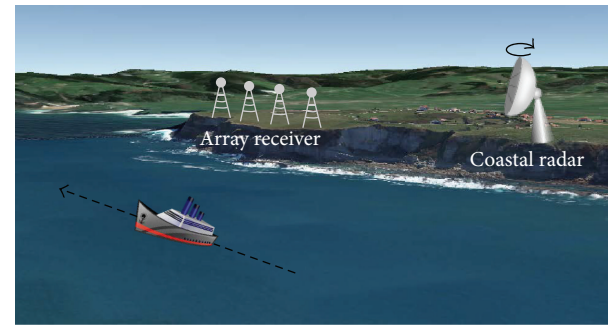

Figure 1: Operative scenario.

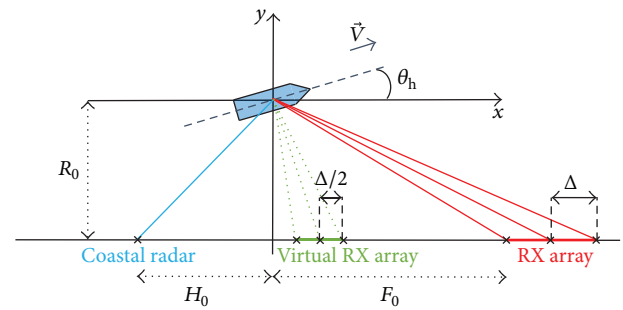

Figure 2: Top view of the system geometry.

The remainder of the paper is organized as follows: Section 2 describes the geometry of the system and the signal model; the receiver array configuration is derived in Section 3 and the data processing in Section 4; simulated results are provided in Section 5 and Section 6 concludes the paper.

2. System Geometry and Echo Model

The operative scenario is depicted in Figure 1. A coastal radar working in X-band (wavelength $\lambda = 3$ cm) monitors the littoral traffic. An array of passive devices is located near the coast, collecting the signal transmitted from the coastal radar and reflected from a moving ship. The ship is modeled as a rigid body in the far field characterized by K dominant scattering centers with complex reflectivity constant along the length of synthetic aperture. The ship is assumed moving with translation motion and negligible rotations (i.e., low sea-state conditions).

The geometry of the system is depicted in Figure 2. For the sake of simplicity in the subsequent derivation, we consider the elements of the array receiver and the coastal radar aligned along the x direction. Within this reference system, coastal radar coordinates are given by

$$\begin{aligned} x_{\mathrm{TX}} &= -H_0, \\ y_{\mathrm{TX}} &= -R_0, \\ z_{\mathrm{TX}} &= Z_{\mathrm{T}}. \end{aligned} \tag{1}$$

Let N be the number of elements of the array and Δ the interelement distance, and the nth receiving element position ($n = 1, \ldots, N$) is

$$\begin{aligned} x_{\mathrm{RX}^n} &= F_0 + (n-1)\,\Delta, \\ y_{\mathrm{RX}^n} &= -R_0, \\ z_{\mathrm{RX}^n} &= Z_{\mathrm{R}}. \end{aligned} \tag{2}$$

The coastal radar illuminates the target each T_{scan} seconds, whose value depends on the rotation speed of its antenna. Let M be the number of processed scans and let $\vec{V}$ be the target velocity vector, and the kth scatterer position at the mth scan ($m = -M/2, \ldots, M/2 - 1$) is given by

$$\begin{aligned} x_k(m) &= x_k^0 + \left|\vec{V}\right| \cos(\theta_{\mathrm{h}})\, mT_{\mathrm{scan}}, \\ y_k(m) &= y_k^0 + \left|\vec{V}\right| \sin(\theta_{\mathrm{h}})\, mT_{\mathrm{scan}}, \end{aligned} \tag{3}$$

where θ_{h} is the target heading angle and (x_k^0, y_k^0) are the scatterer coordinates at the central scan instant.

Without loss of generality, we assume the target reference point located in $(x_0^0, y_0^0) = (0, 0)$. For such a scatterer, the signal received from the nth array element during the mth scan is given by

$$s_0(m,n) = A_0 \cdot \exp\left\{-j\frac{2\pi}{\lambda}\left[R_{\mathrm{TX}}(m) + R_{\mathrm{RX}^n}(m)\right]\right\}, \tag{4}$$

where $R_{\mathrm{TX}}(m)$ and $R_{\mathrm{RX}^n}(m)$ are the target to transmitter and target to nth receiver distances, respectively, and A_0 is its complex amplitude. By expanding the bistatic ranges in (4) in Taylor series and stopping at second order, we obtain

$$\begin{aligned} s_0(m,n) \cong A_0 \cdot \exp\Bigg\{-j\frac{2\pi}{\lambda}\Bigg[&\left(\sigma_{\mathrm{TX}} + \sigma_{\mathrm{RX}^n}\right) \\ &+ \left(\alpha_{\mathrm{TX}} + \alpha_{\mathrm{RX}^n}\right) \cdot mT_{\mathrm{scan}} + \frac{1}{2}\left(\beta_{\mathrm{TX}} + \beta_{\mathrm{RX}^n}\right) \\ &\cdot \left(mT_{\mathrm{scan}}\right)^2\Bigg]\Bigg\}. \end{aligned} \tag{5}$$

Let $V_x = |\vec{V}|\cos(\theta_{\mathrm{h}})$ and $V_y = |\vec{V}|\sin(\theta_{\mathrm{h}})$ be the target velocity components along the x and y directions, respectively, and the polynomial phase coefficients in (5) are as follows:

$$\begin{aligned} \sigma_{\mathrm{TX}} &= \sqrt{H_0^2 + R_0^2 + Z_{\mathrm{T}}^2}, \\ \sigma_{\mathrm{RX}^n} &= \sqrt{\left(F_0 + (n-1)\,\Delta\right)^2 + R_0^2 + Z_{\mathrm{R}}^2}, \\ \alpha_{\mathrm{TX}} &= \frac{H_0 V_x + R_0 V_y}{\sigma_{\mathrm{TX}}}, \\ \alpha_{\mathrm{RX}^n} &= \frac{-\left(F_0 + (n-1)\,\Delta\right) V_x + R_0 V_y}{\sigma_{\mathrm{TX}}}, \\ \beta_{\mathrm{TX}} &= \frac{\left(H_0 V_y + R_0 V_x\right)^2}{\sigma_{\mathrm{TX}}^3}, \\ \beta_{\mathrm{RX}^n} &= \frac{\left(\left(F_0 + (n-1)\,\Delta\right) V_y + R_0 V_x\right)^2}{\sigma_{\mathrm{RX}^n}^3}. \end{aligned} \tag{6}$$

It is worth to explicitly notice that in practice the altitudes of both transmitter and receiving array, Z_{T} and Z_{R}, respectively, are considerably lower than the target distance. Consequently, the only effect of the difference among the transmitter, receiver, and target heights is a slight difference between the ground plane and the image (i.e., slant) plane. Therefore, in the following for the sake of clearness we refer to the coplanar geometry.

Finally from (5)-(6), it is easy to obtain the expression of the received signal from the kth scatterer $s_k(m,n)$ by replacing H_0 with $H_k = H_0 + x_k^0$, F_0 with $F_k = F_0 - x_k^0$, and R_0 with $R_k = R_0 + y_k^0$.

3. Design of the Array

In order to design the array, we have to set the number of its elements and their distances. The configuration has to allow obtaining an ISAR image of the ship with proper cross-range resolution. The achievable cross-range resolution ρ_{cr} depends on the overall view angle $\Delta\theta$ observed during the aperture time T_{a} [9]:

$$\rho_{\mathrm{cr}} = \frac{\lambda}{2\Delta\theta}. \tag{7}$$

For a target at distance R_0 moving with velocity component V_x along the x direction, $\Delta\theta$ is given by

$$\Delta\theta = \frac{T_{\mathrm{a}}\left|V_x\right|}{R_0}. \tag{8}$$

In the framework of coastal surveillance, typical speeds of the targets of interest are in the order of 1–20 kt and the range is in the order of tens of kilometers. It is easy to verify that we need aperture times in the order of ten seconds to reach resolution values suitable to provide images to be employed in ATR procedures. Since the radar antenna rotates with speed of about 10–30 rpm, T_{scan} is 2–6 s, and hence we need to observe the target for M successive scans. Therefore, in order to obtain a desired value ρ_{cr} of cross-range resolution, we need to form a synthetic aperture over a number of scans given by

$$M = \frac{\lambda R_0}{2\rho_{\mathrm{cr}} T_{\mathrm{scan}}\left|V_x\right|}. \tag{9}$$

The Doppler bandwidth provided by the target can be written as

$$B_{\mathrm{d}} = \frac{4\left|V_x\right|}{\lambda}\sin\left(\frac{\Delta\theta}{2}\right) \approx \frac{2\left|V_x\right|\Delta\theta}{\lambda} = \frac{\left|V_x\right|}{\rho_{\mathrm{cr}}}. \tag{10}$$

Its inverse is the sampling period requested by the Nyquist theorem. Through its rotations, the coastal radar operates a sampling of the signal with a period equal to T_{scan}, which is greater than $\rho_{\text{cr}}/|V_x|$ for practical situations. For example, if we aim at obtaining a resolution of 2 m for a target moving with tangential velocity 2.5 m/s (≈5 kt), T_{scan} should be 0.8 s that would require the antenna rotating with a speed of 75 rpm, much greater than the rotation speeds commonly employed by coastal radars.

Nevertheless, due to their physical distance, the $(n+1)$th element of the array will receive the samples with a delay with respect to the nth element, and this delay is given by

$$\tau = \frac{1}{2}\frac{\Delta}{|V_x|}. \tag{11}$$

In the above equation, the coefficient 1/2 is due to the bistatic geometry of the system. Indeed, since a bistatic acquisition is equivalent to a monostatic acquisition located on the bisector between the transmitter and receiver line-of-sights [12–14], a virtual array of N elements having interelement spacing equal to half of the physical distance is achieved; see Figure 2.

Since the Nyquist theorem requires $\tau \leq B_{\text{d}}^{-1}$, we have to impose a maximum distance between the elements of the array; by carrying out the calculus, from (9), (10), and (11) we found that Δ has to be at least twice the desired cross-range resolution:

$$\Delta \leq \frac{\lambda R_0}{MT_{\text{scan}}|V_x|} = 2\rho_{\text{cr}}. \tag{12}$$

Therefore, we can set $\Delta = 2\rho_{\text{cr}}/\mu$, where $\mu \geq 1$.

As previously discussed, in order to increase the azimuth resolution, the target is observed for M successive scans. This imposes the time interval ΔT covered by the array during the single-scan to be at least equal to T_{scan}, thus avoiding gaps between successive scans. ΔT is N times τ, and therefore, from (9) and (11)

$$N\tau \geq T_{\text{scan}} \Longrightarrow N \geq \left\lceil 2\mu M \frac{T_{\text{scan}}^2 |V_x|^2}{\lambda R_0} \right\rceil, \tag{13}$$

where $\lceil(\cdot)\rceil$ is the ceil operator needed to have an integer number of elements. From (12) and (13) we get the physical extension of the array; that is,

$$L_{\text{A}} = N\Delta = 2T_{\text{scan}}|V_x|. \tag{14}$$

Finally, to complete the design of the array the value of μ has to be set. The condition $\mu = 1$ represents the less demanding configuration for the array, since it corresponds to having the minimum number of elements separated as much as possible. Nevertheless, the interelement distance affects the nonambiguous azimuth swath W. Indeed, the angular sampling $\delta\theta$ is given by $\Delta/2R_0$, and from (9) and (12) we obtain

$$W = \frac{\lambda}{2\delta\theta} = \mu MT_{\text{scan}}|V_x| = \mu L_{\text{s}}, \tag{15}$$

$L_{\text{s}} = MT_{\text{scan}}|V_x|$ being the length of the synthetic aperture. In the event that, for a given Δ value, N is the minimum number of elements, $L_{\text{s}} = (\Delta/2)MN$, where the ceil operator in (13) has been neglected. Let D be the maximum size of the ship along the cross-range dimension; it must be

$$\mu \geq \frac{D}{L_{\text{s}}}. \tag{16}$$

As an example, let us consider a ship moving with $|\vec{V}| = 5$ m/s along the positive x direction at a distance $R_0 = 10$ km. A coastal radar with a scan rate of 20 rpm (corresponding to $T_{\text{scan}} = 3$ s) detects and tracks the ship. We aim at obtaining an ISAR image of such target with $\rho_{\text{cr}} = 2.5$ m. To the purpose, we need $M = 4$ scans, (9), and the receiving array has to be composed by elements at a distance of $5/\mu$ meters. By setting $\mu = 1$ and choosing for N the minimum allowed value, we obtain an array of 6 elements at a distance of 5 m. In such conditions, the array is able to correctly sample the signal over the whole aperture time, and by the proper processing of the data (addressed in the following section), the ISAR image can be obtained. However, the choice $\mu = 1$ entails an azimuth swath equal to 60 m and target with size larger than such a value will suffer from aliasing effects. If $D = 100$ m, we have to set $\mu \geq 1.67$ to have a sufficient large swath. For example, by setting $\mu = 2$, we obtain an array of 12 elements with interelement distance 2.5 m able to image unambiguously target of maximum length 120 m at 10 km range.

As it has been shown by the above equations, for given transmitter parameters of the coastal radar, the array design depends on the parameters of the target, specifically on its distance from the radar system R_0 and on its tangential velocity $|V_x|$. Obviously, the array has to be designed in order to fulfill the imaging requirements for the most demanding cases, represented by the shorter distance and the faster target. Let $|\vec{V}| = 10$ m/s (≈20 kt) be the maximum speed considered for the ship targets of interest, and suppose the system surveying a large corridor going from $R_{\text{min}} = 4$ km till $R_{\text{max}} = 20$ km range. Furthermore, we assume a maximum extent of the ship $D = 100$ m. Figure 3 shows the main parameters of the array for the different distance and tangential velocity couples for the case of a coastal radar with $T_{\text{scan}} = 3$ s. As we expected, the maximum number of elements at the lowest interelement distance is obtained for the target moving at the maximum speed and at the minimum distance at the same time. In such a situation, we have to configure an array with 50 elements with spacing 1.2 m.

Let us now consider a target moving at a distance greater than R_{min}. Since $W = \lambda R_0/\Delta$, a larger azimuth swath will be obtained, therefore allowing to correctly image targets with $D > 100$ m. On the other hand, for a given target velocity and number of integrated scans, a worse resolution is obtained, (7) and (8). However, by increasing the number of integrated scans, desired resolution values can be reached.

Then, we analyze the case of a target moving with a velocity lower than the maximum considered value for which the array has been configured. As it has been previously discussed, the delay experienced by two adjacent elements of the array is related to the tangential velocity of the target, (11), and during a scan, the array covers a time interval equal to $N\tau$. In the event that $\Delta T = N\tau > T_{\text{scan}}$, during the $(m+1)$th

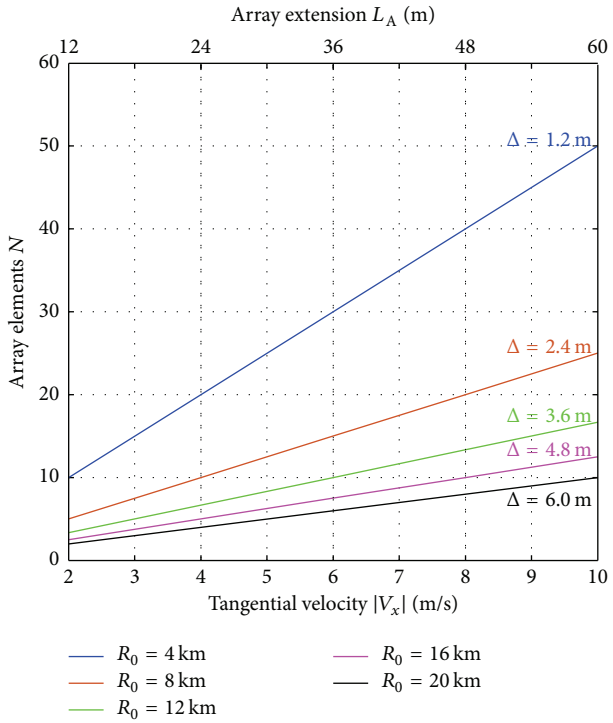

FIGURE 3: Array parameters as a function of the target parameters (T_{scan} = 3 s).

scan the last elements of the array are still receiving the target contributions due to the transmissions carried out at the mth scan. Therefore, as it has been sketched in Figure 4, in the time domain an overlapping between signals received by the array during successive scans will occur. Specifically, let N_{eq} be the number of elements such that $N_{eq}\tau = T_{scan}$, the signals received by the last $(N - N_{eq})$ elements of the array during the mth scan overlap in time with the signals received by the first N_{eq} elements of the array during the $(m + 1)$th scan. Consequently, in order to achieve a contiguous sampling of the azimuth signal over $M > 1$ scans, only the first N_{eq} elements of the array should be considered. It should be pointed out that, in general, N_{eq} is not an integer number, and a fractioned number of elements of the array should be selected. Such a problem can be faced by carrying out a proper interpolation of the data, as it will be detailed in describing the array data processing.

4. Array Data Processing

In this section, we present the processing of the data received from the array to achieve the ISAR image of the target. Section 4.1 deals with the case of a monodimensional azimuth signal. The objective of the subsection is to illustrate the proof of concept and highlight the main operations involved in the azimuth compression. Based on the concepts illustrated in Section 4.1, the focusing technique for a distributed target is detailed in Section 4.2.

4.1. Monodimensional Azimuth Signal Proof of Concept. Let us assume a single scatterer located in (x_k^0, y_k^0) at the reference time, and suppose we aim at focusing it as observed in a single scan. To the purpose, we need to compensate the phase shift of the target as it moves through the aperture. Due to the geometry of the system, we have two contributions. The former is due to the transmitter-target distance, and it is the same for all the elements of the receiving array. The latter is due to the target-receiver distance, and it varies with the element index. The azimuth compression is therefore obtained by multiplying the data received by each element of the array for the complex conjugate of a common reference signal given by

$$s_{TX}^{ref} = \exp\left\{-j\frac{2\pi}{\lambda}\left[a_0 + a_1 mT_{scan} + \frac{a_2}{2}(mT_{scan})^2\right]\right\} \quad (17)$$

and then, for the nth element, by multiplying the data for the complex conjugate of the reference signal given by

$$s_{RX^n}^{ref} = \exp\left\{-j \cdot \frac{2\pi}{\lambda}\left[b_0^{(n)} + b_1^{(n)} mT_{scan} + \frac{b_2^{(n)}}{2}(mT_{scan})^2\right]\right\}. \quad (18)$$

The coefficients $(a_0, \ldots, a_2, b_0^{(n)}, \ldots, b_2^{(n)})$ are the coefficients of the Taylor expansion of the bistatic distances for the scatterer located in $(x_0^0 = 0, y_k^0)$, which can be obtained from (6) by replacing R_0 with $R_k = R_0 + y_k^0$. Thereby, the compensation of the linear phase terms will result in a residual Doppler centroid related to the kth scatterer position in the azimuth domain. It should be also pointed out that, as usual in ISAR processing, we neglect the variation of the Doppler rate with the cross-range position of the scatterer while, as stated above, we take into account its variation along the range direction. Then, by applying a FFT the scatterer ISAR profile can be obtained.

Now, we aim at focusing the target observed over a number of successive scans. As discussed in Section 3, in general the data received by the array during successive scans overlap in time, and the selection of the first N_{eq} elements of the array must be performed. Since such a number being an integer number cannot be ensured, a proper interpolation of the data must be performed in order to artificially increase the time sampling. This task can be easily accomplished by zero padding. After the data corresponding to the mth scan have been compressed by multiplying the array data for the reference signals (17) and (18), a zero padding is performed in the frequency domain. Let q be the oversampling factor and the sampling time is τ/q; for q values high enough, we can assume $qN_{eq} \cong \lceil qN_{eq} \rceil$, and therefore a more precise selection of the data can be performed, thus ensuring a contiguous time observation among successive scans. After the time oversampling and selection of the data have been performed, vector signals $\mathbf{s}_m^{int}$ with dimension $[1 \times qN_{eq}]$ can be obtained by interleaving the data corresponding to each scan. Two different strategies could be adopted to merge the data received over the successive scans to provide the increased cross-range resolution. The former operates in the time domain and it

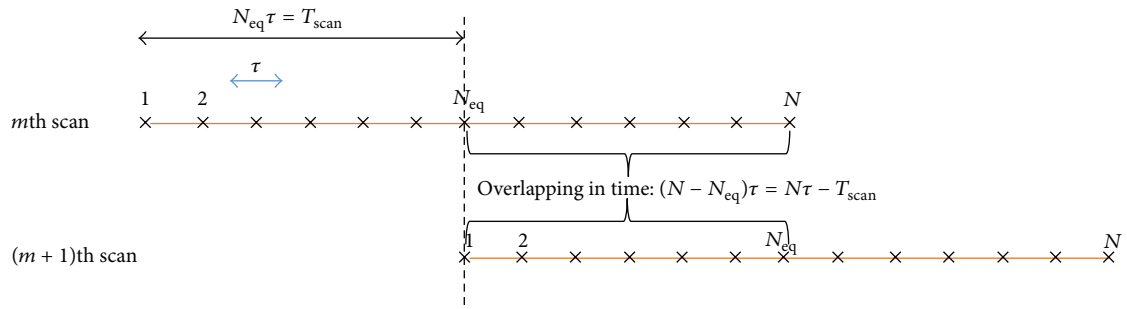

Figure 4: Time intervals covered by the array over successive scans.

consists in placing side by side the single-scan data to obtain the final vector $\mathbf{s}_{\mathrm{TOT}}^{\mathrm{int}} = [\mathbf{s}_1^{\mathrm{int}}, \ldots, \mathbf{s}_M^{\mathrm{int}}]$; a FFT can be subsequently applied thus obtaining the multiscan ISAR profile.

The latter strategy operates in the frequency domain. The single-scan ISAR profile can be obtained by applying a FFT to each $\mathbf{s}_m^{\mathrm{int}}$ after they have been temporarily aligned. To this purpose, for each scan a FFT can be applied to the vector $\tilde{\mathbf{s}}_m^{\mathrm{int}} = [\mathbf{z}_m^{\mathrm{left}}, \mathbf{s}_m^{\mathrm{int}}, \mathbf{z}_m^{\mathrm{right}}]$, where $\mathbf{z}_m^{\mathrm{left}}$ and $\mathbf{z}_m^{\mathrm{right}}$ are zero vectors with dimensions $[1 \times qN_{\mathrm{eq}}(m-1)]$ and $[1 \times qN_{\mathrm{eq}}(M-m)]$, respectively. Then, by coherent summation of the single-scan profiles, the multiscan ISAR profile is obtained.

So far, we considered completely negligible target rotations. This is reasonable in our hypothesis of low sea-state conditions, and the imaging of rotating ships could be addressed by conventional ISAR techniques or by using formations of active and passive radar sensors to reach high resolution products [13, 14]. Nevertheless, even though they are limited, rotations may affect the imaging technique here proposed. Therefore, the case in which the target motion is characterized also by rotations is here discussed. In the case of a jointly translating and rotating target, kth scatterer coordinates (3) can be rewritten in matrix notation as

$$\begin{bmatrix} x_k(m) \\ y_k(m) \end{bmatrix} = \begin{bmatrix} x_k^0 \\ y_k^0 \end{bmatrix} \begin{bmatrix} \cos(\omega m T_{\mathrm{scan}}) & \sin(\omega m T_{\mathrm{scan}}) \\ -\sin(\omega m T_{\mathrm{scan}}) & \cos(\omega m T_{\mathrm{scan}}) \end{bmatrix} + \begin{bmatrix} V_x m T_{\mathrm{scan}} \\ V_y m T_{\mathrm{scan}} \end{bmatrix}, \tag{19}$$

where ω is the rotation speed. By carrying out the calculus, we can write scatterer coordinates as

$$\begin{aligned} x_k(m) &= \left\{x_k^0 \left[\cos(\omega m T_{\mathrm{scan}}) - 1\right] + y_k^0 \sin(\omega m T_{\mathrm{scan}})\right\} + \left\{x_k^0 + V_x m T_{\mathrm{scan}}\right\} = x_k^V(m) + x_k^\omega(m), \\ y_k(m) &= \left\{y_k^0 \left[\cos(\omega m T_{\mathrm{scan}}) - 1\right] - x_k^0 \sin(\omega m T_{\mathrm{scan}})\right\} + \left\{y_k^0 + V_y m T_{\mathrm{scan}}\right\} = y_k^V(m) + y_k^\omega(m) \end{aligned} \tag{20}$$

x_k^V and y_k^V being the target coordinates for the only-translating target and x_k^ω and y_k^ω the shifts due to the rotation.

As pointed out, the dwell time during a single scan is due to the ratio between the antenna beamwidth and the scan rate. For example, an antenna with rotation rate of 20 rpm and beamwidth 0.6° provides a time-on-target of 5 ms. In such a limited interval, target rotation can be neglected and therefore the rotations do not affect the imaging processing within a single scan. Nevertheless, the rotation causes a Doppler shift experienced by the data received among the successive scans, deriving from the different orientations of the target. Such a Doppler shift can be written as

$$\Delta f_k(m) = \frac{2}{\lambda} \frac{V_x}{R_0} \delta_k^{\mathrm{cr}}(m), \tag{21}$$

where $\delta_k^{\mathrm{cr}}(m)$ represents the cross-range shift due to the difference in cross-range position with respect to the nominal position accounting only for the translation; that is, $\delta_k^{\mathrm{cr}}(m) = x_k^\omega(m)$. The compensation of this Doppler shift corresponds to performing a coregistration among the single-scan responses, which can be obtained by multiplying $\tilde{\mathbf{s}}_m^{\mathrm{int}}$ for a phase ramp $\exp\{j2\pi\Delta f_k(m)\tilde{\mathbf{n}}\}$, $\tilde{\mathbf{n}}$ being the vector of time instants going from $-(M/2)T_{\mathrm{scan}}$ to $(M/2)T_{\mathrm{scan}}$ with step $(1/q)(\Delta/2|V_x|)$.

Furthermore, the rotation causes a different range of the scatterer with respect to the one foreseen by the translational motion only. Such a difference in range entails phase jumps among the different scans to be compensated. Therefore, the single-scan data $\tilde{\mathbf{s}}_m^{\mathrm{int}}$ have to be further multiplied by a term given by

$$\Delta\xi_k(m) = \exp\left\{\frac{j2\pi}{\lambda}\delta_k^{\mathrm{r}}(m)\right\} \tag{22}$$

with $\delta_k^{\mathrm{r}}(m) = y_k^\omega(m)$.

4.2. Focusing Technique for Distributed Target. In previous section, we considered the case of a monodimensional signal in order to illustrate the main concept to obtain the multiscan ISAR profile. It has been shown that the crucial steps are azimuth dechirping, time selection, time alignment, and possible rotation compensations. Based on these considerations, the focusing technique for a distributed target is developed as depicted in Figure 5. It comprises two parts: first, data received by the array during each scan are processed; then,

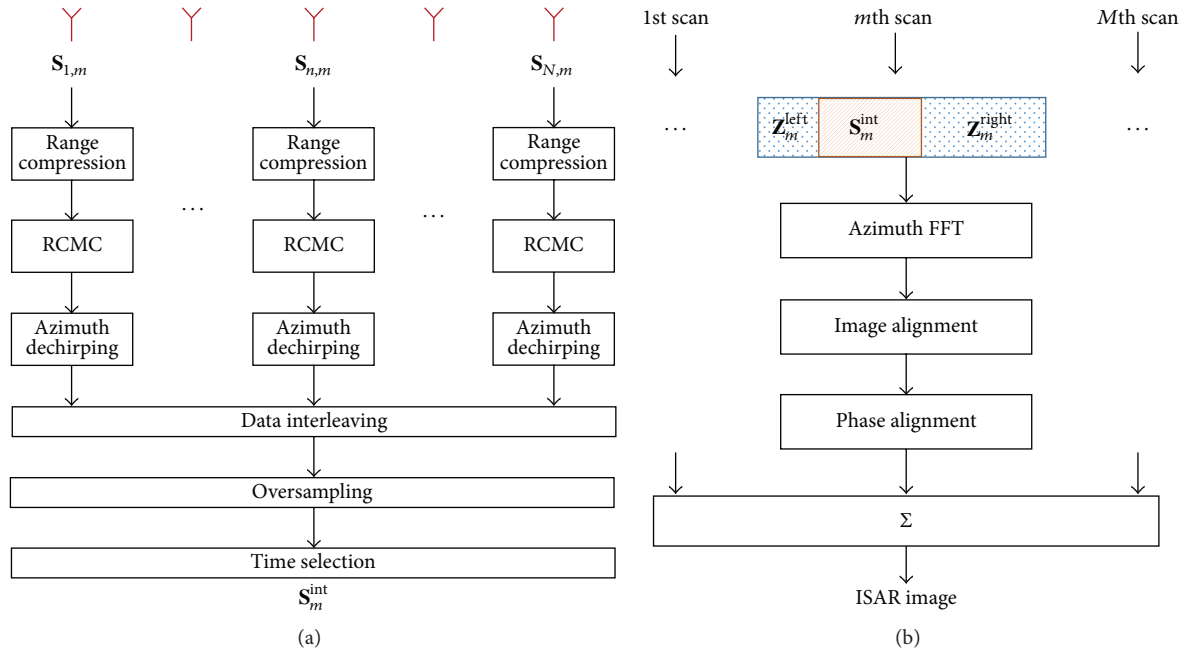

Figure 5: Processing scheme: (a) single-scan processing and (b) multiscan data fusion.

data received during multiple scans are merged to form the final image.

Accounting also for the fast time dimension, the data received from the nth sensor during the mth scan are organized in a matrix $\mathbf{S}_{n,m}$, with number of rows equal to the number of fast time samples and number of columns depending on the number of samples within the time-on-target. Taking into account the short duration of the time-on-target, we can neglect the variation among adjacent pulses collected by a single array element during a scan and therefore, for sake of simplicity, we assume that the nth receiver collects a single sample during the mth time-on-target for each range bin. Therefore, $\mathbf{S}_{n,m}$ is a column vector of dimension $[L \times 1]$, L being the number or range bins. The processing of the data received by the array during the mth scan consists of the following steps (see Figure 5(a)):

(1) Range compression: allowing transiting in the slant range domain.

(2) Range Cell Migration Correction (RCMC): due to the long integration time, the correction of the range migration is a needed step. It can be obtained in the fast frequency domain by multiplying the Fourier transformed data by a reference signal equal to $\exp\{j2\pi f_r(\delta R_n^0(m)/c)\}$. f_r is the fast frequency, c is the speed of light, and $\delta R_n^0(m)/c$ is the time delay due to the variation of the distance between the target reference point and the central element of the array at the reference scan $m = 0$ and the distance between the target reference point and the nth array element at the mth scan.

(3) Azimuth dechirping: for the lth range bin, two reference signals as in (17) and (18) are generated, where the coefficients $(a_0, \ldots, a_2, b_0^{(n)}, \ldots, b_2^{(n)})$ account for the specific range bin position; namely, as explained in Section 4.1, in the Taylor coefficients (6) we have to replace R_0 with $R_0 + \overline{y}_l$, $\overline{y}_l$ being the lth value of the range axis.

(4) Data interleaving among the array elements: to obtain a data matrix $\mathbf{S}_m^{\text{int}}$ of dimension $[L \times N]$.

(5) Oversampling: as explained in the previous subsection, by means of Fourier transform and zero padding, an increased time sampling is obtained, and after the oversampling $\mathbf{S}_m^{\text{int}}$ has dimension $[L \times qN]$.

(6) Time selection: to ensure time continuity among the data collected by the successive scans, the first qN_{eq} columns of $\mathbf{S}_m^{\text{int}}$ are selected. After this operation, $\mathbf{S}_m^{\text{int}}$ has dimension $[L \times qN_{\text{eq}}]$. It should be pointed out that if the interest is in focusing the image resulting from a single scan, time selection can be bypassed, and through an azimuth FFT the single-scan image can be obtained.

At this point, M matrices $\mathbf{S}_m^{\text{int}}$ are available covering a time interval equal to MT_{scan}. The following operations are performed to obtain the multiscan ISAR image (see Figure 5(b)):

(1) Time shift: as explained in Section 4.1, for temporarily aligning the data received by each scan, the array data processed for the mth scan can be organized in the matrix $[\mathbf{Z}_m^{\text{left}}, \mathbf{S}_m^{\text{int}}, \mathbf{Z}_m^{\text{right}}]$, $\mathbf{Z}_m^{\text{left}}$ and $\mathbf{Z}_m^{\text{right}}$ being zero matrixes with dimension $[L \times qN_{\text{eq}}(m-1)]$ and $[L \times qN_{\text{eq}}(M-m)]$, respectively.

(2) Single-scan images formation: by applying a FFT along the azimuth dimension, the ISAR image corresponding to the mth scan is achieved. Thanks to

the time-shift operation, the images correspond to the same time interval, and, in the event that rotation motion can be neglected, a coherent summation provides the ISAR image with M times finer (with respect to the single-scan images) cross-range resolution. However, since, in general, ship targets undergo rotations, their effects have to be compensated as explained in steps (3) and (4).

(3) Image coregistration: the short duration of the time-on-target allows considering each single-scan image as a "snapshot" of the target, and the possible rotation motion does not affect the imaging processing [15]. However, such a rotation motion causes the target to change its orientation when imaged at different scans, and hence the series of single-scan images can be regarded as snapshots of the same target that has changed its orientation. Therefore, a rotation of the mth scan image accordingly to an angle equal to $\omega m T_{\text{scan}}$ has to be performed. It should be pointed out that such an image alignment also compensates the Doppler shift (21) experienced by each scatterer.

(4) Phase alignment: as it is shown by (22), the kth scatterer of the scene undergoes a phase jump when imaged in different scans, and, since $\delta_k^{\text{r}}(m) = y_k^{\omega}(m)$ is a function of both cross-range and range positions, (20), a space variant phase compensation has to be performed. Let $\overline{y}_l$ be the lth range bin value and let $\overline{x}_h$ be the hth cross-range bin value; for the mth scan a phase matrix with elements $\Delta\xi_{l,h}(m) = \exp\{(j2\pi/\lambda)\delta_{l,h}^{\text{r}}(m)\}$, with $\delta_{l,h}^{\text{r}}(m) = \overline{y}_l[\cos(\omega m T_{\text{scan}}) - 1] - \overline{x}_h \sin(\omega m T_{\text{scan}})$, can be generated. By multiplying cell by cell the mth scan image for such a matrix, the space variant phase compensation can be accomplished.

(5) Coherent summation: finally, the temporarily aligned, coregistered, and phase aligned single-scan images can be coherently added to form the final multiscan ISAR image.

Finally, it is worth to mention that the described focusing technique accounts for an *a priori* known target motion. Generally, with particular regard to the imaging of noncooperative targets, the motion parameters have to be retrieved directly by the received data, and generally speaking many contributions can be found in the literature dealing with the estimation of the translational and rotational motion of ship targets. Even though the target motion estimation is beyond the goal of this paper, which mainly focuses on the definition of the array parameters and of a suitable processing of the received data, we want here to outline possible strategies to address the issue.

Typically, ISAR requires the compensation of the translational motion between the radar and the target (i.e., motion compensation): largely employed techniques are based on the maximization/minimization of proper cost functions with respect to the unknown translational motion [8], such as the maximization of the contrast [16] or the minimization of the entropy [17]. In our case, the same concept can be adequately applied, where the ship translation can be estimated maximizing the intensity contrast of the set of single-scan ISAR images. In this regard, it is also worth to notice that typical ship translations implicate low terms of the received phase; therefore acceleration and higher order terms could be reasonably neglected for the single-scan autofocusing and do not need to be estimated, thus alleviating the computation burden for this issue.

Regarding the rotational motion, as it has been pointed out in describing the image coregistration procedure, in the proposed system the ship rotations only entail an additional change in the orientation of the ship when imaged in successive scans. The estimation of this additional scan-to-scan rotation can be addressed maximizing proper cost functions on the final image [18] or looking for that angle providing the best alignment among the single-scan images (taking also into account the misalignment due to translation as estimated from the previous step). A promising alternative could be the estimation of the slope of the ship centerline [10], which is a function of the rotation rate as detailed in [19]. Lastly, it is also worth to underline that the proposed imaging technique mainly addresses those scenarios where the low sea-state conditions entail very limited rotations of the ship, thus making the formation of ISAR images with proper resolution hard with conventional techniques. In this work, we accounted for a possible not negligible yaw motion of the ship, since it could also account for an initial target maneuver. In contrast, complicated ship dynamics involving nonnegligible three-dimensional rotations would not require multiple scans and therefore can be treated by resorting to conventional ISAR techniques.

5. Simulated Results

In the simulated analysis, we consider an X-band fully solid state coastal radar for vessel traffic services, operating with a scan rate of 20 rpm and transmitting a chirp signal with a bandwidth of 22 MHz [20]. An array of 50 elements with spacing 1.2 m is configured, allowing imaging targets of maximum length 100 m, at a maximum speed of 10 m/s and at ranges longer than 4 km.

In a first case study, we consider a target moving with velocity $|\vec{V}| = 10$ m/s and heading angle $\theta_{\text{h}} = 60^{\circ}$ at a distance $R_0 = 8$ km, and we consider the target observed over 4 scans. Since $|V_x| = 5$ m/s, during a scan the array covers a time interval twice that of the scan interval, and therefore, to combine the signals received over the successive scans, proper time selection has to be performed. In particular, since $\Delta T = 2T_{\text{scan}}$, in this case $N_{\text{eq}} = (1/2)N$. By considering a single pointlike scatterer located in $(30, 0)$ m at the reference time and applying the processing described in Section 4.1, the cross-range profiles shown in Figure 6 are obtained, when one or more scans have been integrated. As we can observe, cross-range resolution progressively increases by integrating the signals received by the array over an increased number of scans. Specifically, we found $\rho_{\text{cr}} = 8$ m, 6 m, 4 m, 2 m when $M = 1, 2, 3, 4$, respectively, in agreement with the theoretical expectations. It should be pointed out that if a single scan is considered, time selection step could be avoided, and the whole time interval ΔT covered by the array could be

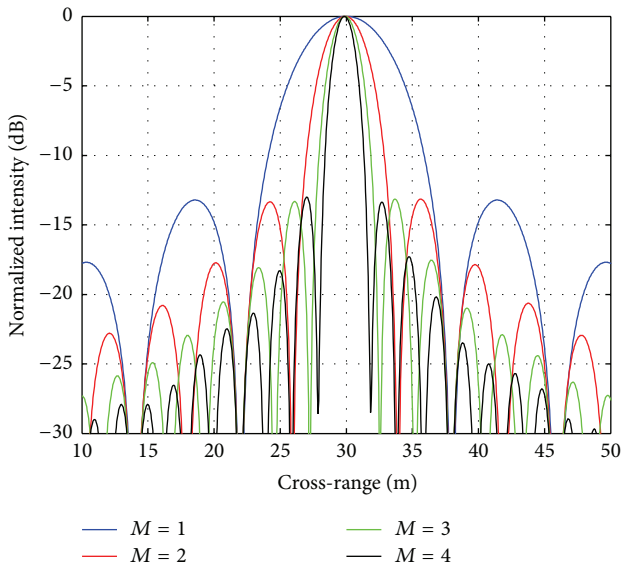

Figure 6: ISAR profiles for successive integrated scans.

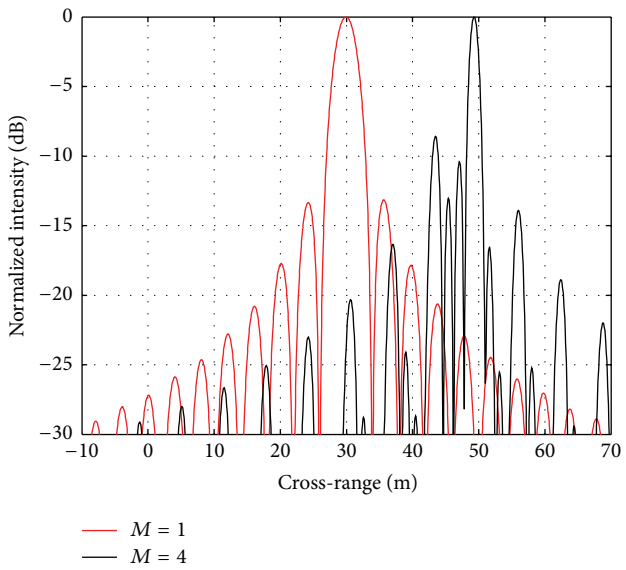

Figure 7: ISAR profiles obtained without applying the time selection.

processed. Since, in this particular scenario, ΔT is twice T_{scan}, the case $M = 1$ without time selection provides the same imaging results as the case $M = 2$ with time selection. Nevertheless, to further increase the resolution by combining $M > 2$ scans, time selection is essential. As example, Figure 7 shows the results obtained without the time selection step for the cases $M = 1$ and $M = 4$. In the former case, we can observe the same profile achieved in Figure 6 for $M = 2$, whereas in the latter, as a consequence of the time overlapping, we observe the scatterer not correctly focused.

The hypothesis of absence of rotation motion is then removed considering the target undergoing a rotation motion with an angular velocity $\omega = 0.5^{\circ}/\text{s}$. We assume the target observed for $M = 3$ scans and we consider an isolated point

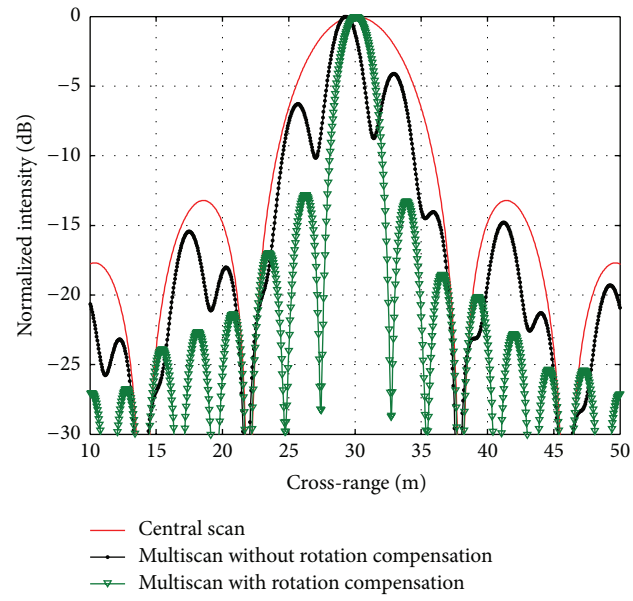

Figure 8: ISAR profiles for nonnegligible rotation motion.

scatterer with coordinates $(30, 10)$ m at the reference time. The ISAR profiles obtained if the effects of the rotational motion have been or have not been taken into account in processing the data are shown in Figure 8. Specifically, red and black plots are the results obtained by focusing the data received when no compensation for the rotation motion has been applied. As we can observe, the rotation has not affected the single-scan imaging result, red plot, whereas a degradation of the quality of the profile (such as wrong position of the peak, higher sidelobes level, and loss in resolution) is experienced for the multiscan case, black plot. By performing a correct image alignment and phase junction steps, successive scan images can be properly combined, and a correct imaging result is obtained, green plot.

Finally, we consider a ship target composed by many pointlike scatterers with different levels of superstructure located at a distance $R_0 = 10$ km and moving with velocity $|\vec{V}| = 7$ m/s and heading angle $\theta_{\text{h}} = -45^{\circ}$. By following the focusing technique described in Figure 5, M single-scan ISAR images of the ships are obtained and then combined to obtain a final multiscan image providing enhanced cross-range resolution. Figure 9 shows the images resulting from the integration of $M = 1, 3, 5$ scans. As we can observe, while the range resolution is limited to be about 6.8 m by the bandwidth of the chirp signal transmitted by the coastal radar, the cross-range resolution of the image increases considering more scans. The single-scan image is shown in Figure 9(a) and we can observe that the poor azimuth resolution (about 10 m) does not allow a proper identification of the main features of the target, such as its size. By considering $M = 3$, Figure 9(b), and $M = 5$ scans, Figure 9(c), we move from 10 m to 3.3 m and to 2 m, respectively. As the azimuth resolution increases, scattering centers not resolvable with the data received during a single scan can be resolved, thus providing enhanced capability to recognize the size of the ship and its main features. For

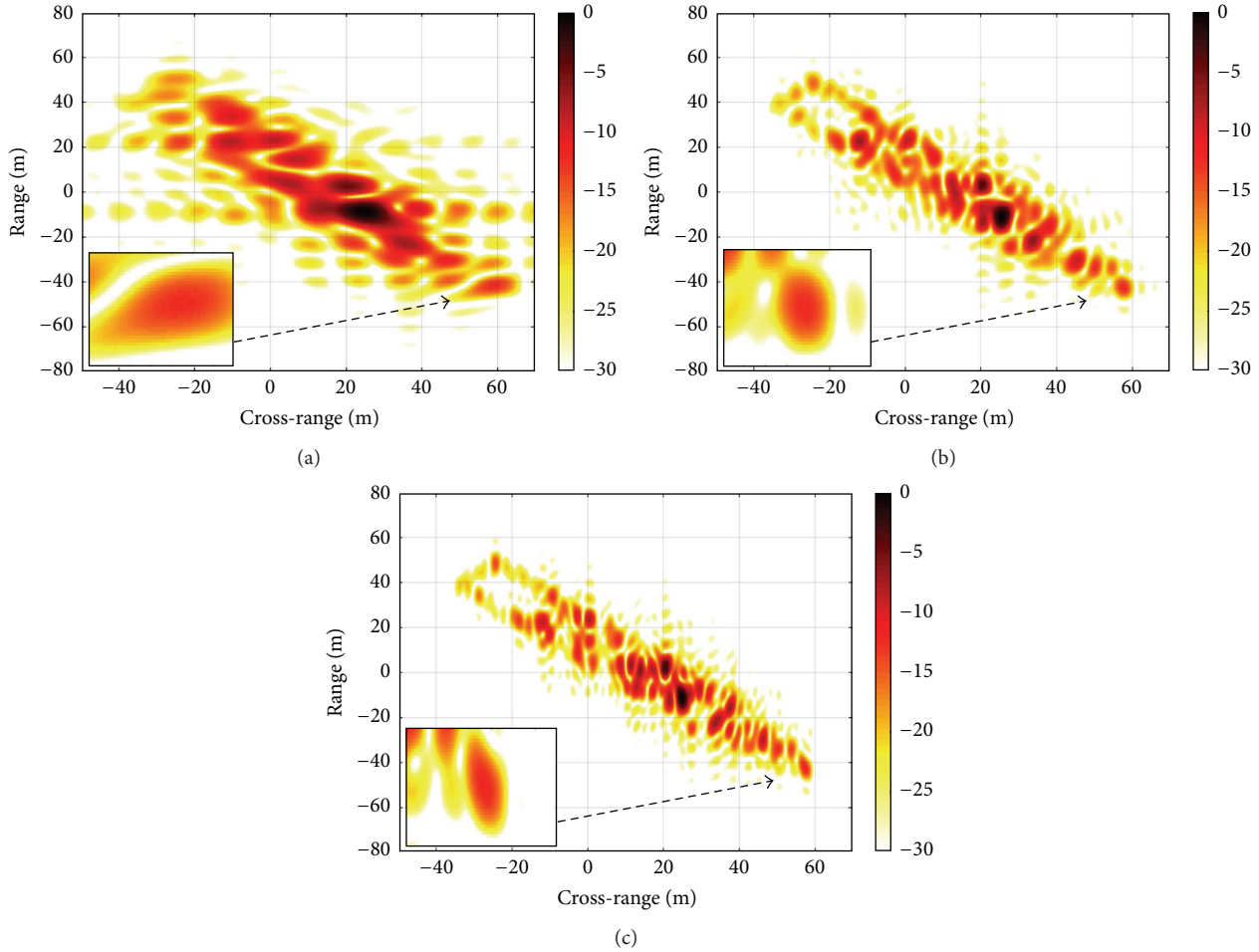

Figure 9: Single/multiscan ISAR images of the ship target.

example, black bottom boxes of Figure 9 highlight the patches of the images corresponding to the bow scatterer, whose position becomes progressively easier to be identified.

6. Conclusions

The paper puts forward a novel ISAR imaging system for coastal surveillance based on a parasitic array receiver and an opportunistic coastal radar. The signal transmitted by a ground-based radar with its antenna rotating for vessel traffic services purposes is exploited as signal of opportunity by an array of passive (receiving only) devices properly located near the coast. The physical aperture provided by such an array, jointly to the synthetic aperture provided by the target motion during successive scans of the radar, allows reaching a Doppler gradient suitable for the image resolution process. Relationships between the parameters of the array and the transmitter parameters have been derived to deal with ship targets of interest. Then, a focusing technique has been proposed able to focus the data collected over one or more scans, even in the case of not negligible rotation motion.

The simulated performance analysis proved the effectiveness of the technique to provide ISAR images of ship targets with suitable resolutions. By exploiting multiple scans, azimuth resolution can be increased, thus achieving cross-range resolutions comparable or even better than the range resolutions, limited by the bandwidth of the transmitted signal. Furthermore, it should be pointed out that because of the exploitation of the translation motion, achievable ISAR images are top views of the ship. Such images can be properly exploited in ATR procedure, thus helping in increasing the efficiency of the vessel traffic monitoring and the coastal surveillance.

Competing Interests

The authors declare that they do not have any conflict of interests.

References

[1] M. Glandrup, "Improving situation awareness in the maritime domain," in *Situation Awareness with System of Systems*, P. van de Laar, J. Tretmans, and M. Borth, Eds., pp. 21–38, Springer, New York, NY, USA, 2013.

[2] D. Pastina, M. Sedhei, and D. Cristallini, "Geostationary satellite based passive bistatic ISAR for coastal surveillance," in

Proceedings of the IEEE Radar Conference, Washington, DC, USA, May 2010.

[3] F. Turin and D. Pastina, "Multistatic passive ISAR based on geostationary satellites for coastal surveillance," in *Proceedings of the IEEE Radar Conference (RadarCon '13)*, Ottawa, Canada, May 2013.

[4] D. W. O'Hagan, A. Capria, D. Petri et al., "Passive Bistatic Radar (PBR) for harbour protection applications," in *Proceedings of the IEEE Radar Conference*, pp. 0446–0450, IEEE, Atlanta, Ga, USA, May 2012.

[5] D. Langellotti, F. Colone, P. Lombardo, M. Sedehi, and E. Tilli, "DVB-T based passive bistatic radar for maritime surveillance," in *Proceedings of the IEEE Radar Conference (RadarCon '14)*, pp. 1197–1202, IEEE, Cincinnati, Ohio, USA, May 2014.

[6] K. Chetty, K. Woodbridge, H. Guo, and G. E. Smith, "Passive bistatic WiMAX radar for marine surveillance," in *Proceedings of the IEEE International Radar Conference*, pp. 188–193, Washington, DC, USA, May 2010.

[7] H. Sun, D. K. P. Tan, Y. Lu, and M. Lesturgie, "Applications of passive surveillance radar system using cell phone base station illuminators," *IEEE Aerospace and Electronic Systems Magazine*, vol. 25, no. 3, pp. 10–18, 2010.

[8] B. D. Steinberg and H. M. Subbaram, *Microwave Imaging Techniques*, Wiley, New York, NY, USA, 1991.

[9] D. R. Wehner, *High-Resolution Radar*, Artech House, Boston, Mass, USA, 2nd edition, 1992.

[10] S. Musman, D. Kerr, and C. Bachmann, "Automatic recognition of ISAR ship images," *IEEE Transactions on Aerospace and Electronic Systems*, vol. 32, no. 4, pp. 1392–1404, 1996.

[11] F. Santi, D. Pastina, and P. Lombardo, "ISAR while-scan mode for coastal surveillance," in *Proceedings of the IEEE Radar Conference (RadarCon '14)*, pp. 1301–1306, Cincinnati, Ohio, USA, May 2014.

[12] B. Correll, "Efficient spotlight SAR MIMO linear collection configurations," *IEEE Journal of Selected Topics in Signal Processing*, vol. 4, no. 1, pp. 33–39, 2010.

[13] D. Pastina, M. Bucciarelli, and P. Lombardo, "Multistatic and MIMO distributed ISAR for enhanced cross-range resolution of rotating targets," *IEEE Transactions on Geoscience and Remote Sensing*, vol. 48, no. 8, pp. 3300–3317, 2010.

[14] D. Pastina, F. Santi, and M. Bucciarelli, "MIMO distributed imaging of rotating targets for improved 2-D resolution," *IEEE Geoscience and Remote Sensing Letters*, vol. 12, no. 1, pp. 190–194, 2015.

[15] G. Hajduch, R. Garello, J.-M. Le Caillec, M. Chabah, and J.-M. Quellec, "High-resolution snapshot SAR/ISAR imaging of ship targets at sea," in *SAR Image Analysis, Modeling, and Techniques V, 39*, vol. 4883 of *Proceedings of SPIE*, March 2003.

[16] F. Berizzi and G. Corsini, "Autofocusing of inverse synthetic aperture radar images using contrast optimization," *IEEE Transactions on Aerospace and Electronic Systems*, vol. 32, no. 3, pp. 1185–1191, 1996.

[17] L. Xi, L. Guosui, and J. Ni, "Autofocusing of ISAR images based on entropy minimization," *IEEE Transactions on Aerospace and Electronic Systems*, vol. 35, no. 4, pp. 1240–1252, 1999.

[18] D. Pastina, "Rotation motion estimation for high resolution ISAR and hybrid SAR/ISAR target imaging," in *Proceedings of the IEEE Radar Conference (RADAR '08)*, pp. 1–6, IEEE, Rome, Italy, May 2008.

[19] D. Pastina and C. Spina, "Slope-based frame selection and scaling technique for ship ISAR imaging," *IET Signal Processing*, vol. 2, no. 3, pp. 265–276, 2008.

[20] F. Amato, M. Fiorini, S. Gallone, and G. Golino, "Fully solid state radar for vessel traffic services," in *Proceedings of the 11th International Radar Symposium (IRS '10)*, pp. 438–441, June 2010.